MICHIGAN STATE UNIVERSITY

CYCLOTRON LABORATORY

ENERGY DEPENDENCE OF FISSION FRAGMENT ANGULAR DISTRIBUTIONS FOR ^{19}F, ^{24}Mg, and ^{28}Si INDUCED REACTIONS on ^{208}Pb

M.B. TSANG, H. UTSUNOMIYA, C.K. GELBKE, W.G. LYNCH,
B.B. BACK, S. SAINI, P.A. BAISDEN and M.A. McMAHAN

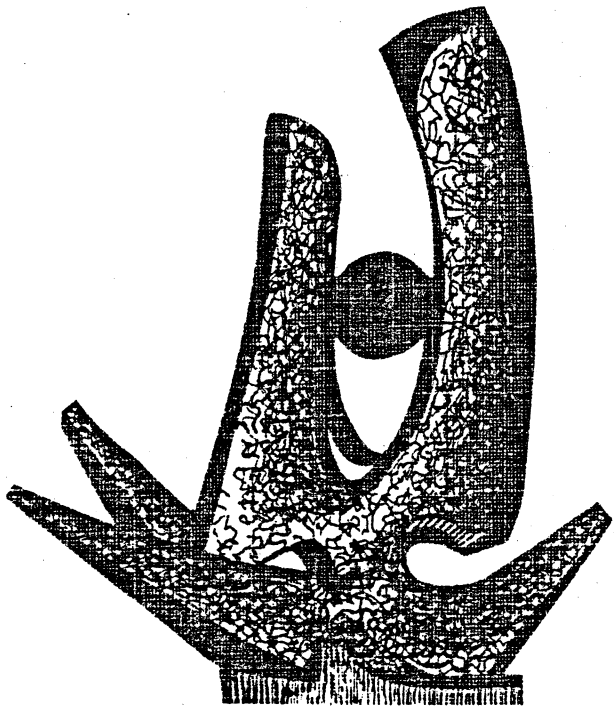

MAY 1983

MSUCL-412

MSUCL-412
May 1983

ENERGY DEPENDENCE OF FISSION FRAGMENT ANGULAR DISTRIBUTIONS FOR ^{19}F, ^{24}Mg AND ^{28}Si INDUCED REACTIONS ON ^{208}Pb

M.B. Tsang, H. Utsunomiya, C.K. Gelbke, and W.G. Lynch
National Superconducting Cyclotron Laboratory, Michigan State University, East Lansing, Mi.48824

B.B. Back and S. Saini
Chemistry Division, Argonne National Laboratory, Argonne, Il. 60439

P.A. Baisden, and M.A. McMahan
Nuclear Chemistry Division, Lawrence Livermore National Laboratory, Livermore, Ca. 94558

Abstract

The energy dependence of fission fragment angular distributions was measured for reactions induced by ^{19}F, ^{24}Mg, and ^{28}Si on ^{208}Pb over the range of incident energies of E/A = 5.6 - 10 MeV. For all three systems the angular distributions are inconsistent with the saddle point deformations of the rotating liquid drop model.

Within the framework of the transition state theory for nuclear fission [1,2], the angular distributions of fission fragments depend on the saddle point deformation, angular momentum and excitation energy of the parent nucleus. With few exceptions, present experimental information [2,3] is essentially consistent with the saddle point deformations predicted by the liquid drop model [4,5]. Clear discrepancies with these saddle point deformations have recently been reported [6-8] for ^{32}S induced reactions on targets of Au, Pb, Th, U, and Cm, whereas no such discrepancies were detected [6,7] for ^{16}O induced reactions on Bi and U. These findings are difficult to understand in terms of the concept of fission decay of the compound nucleus and have been interpreted as due to the occurrence of fast fission processes for ^{32}S induced reactions [7]. In order to obtain more systematic information about the systematic trends of fission fragment angular distributions observed in heavy ion induced reactions, we investigated ^{19}F, ^{24}Mg, and ^{28}Si induced reactions on ^{208}Pb over the range of incident energies of E/A = 5.6 - 10 MeV.

The experiment was performed at the superconducting linear postaccelerator at Argonne National Laboratory. A ^{208}Pb target of 0.2 mg/cm^2 areal density was used. Except for the larger number of detectors used in the present experiment, the experimental technique was identical to the one described in ref.8. The absolute normalization of the cross sections is accurate to within 7 % . Contributions

from sequential fission following deeply inelastic reactions are negligible in all cases.

The fission fragment angular distributions measured in the present experiment are shown in Figure 1. Similar to previous measurements for ^{32}S induced reactions on ^{208}Pb, larger angular anisotropies are observed at higher incident energies. The angle integrated fission cross sections and the corresponding sharp cut off angular momenta for capture are given in Table 1.

We assume that the final helicity distribution of the fission fragments reflects a statistical equilibrium distribution at some intermediate stage of the reaction; this "transition state" is generally identified with the saddle point [2] if the reaction proceeds via formation of an equilibrated compound nucleus. For first chance fission following the capture of spin - zero projectile and target nuclei, the expression for the angular distributions is given by

$$\frac{d\sigma}{d\Omega}(\theta) = \pi\lambda\!\!\!^{-2} \sum_{\ell=0}^{\infty} (2\ell+1)\, T_\ell \;\; \frac{\sum_{K=-\ell}^{+\ell} \tfrac{1}{2}\,(2\ell+1)\, |\mathcal{D}^{\ell}_{M=0,K}(\theta)|^2 \exp\left(-\frac{K^2}{2K^2_{0,\ell}}\right)}{\sum_{K=-\ell}^{+\ell} \exp\left(-K^2/2K^2_{0,\ell}\right)} \qquad (1)$$

with

$$K^2_{o,\ell} = T\,\mathcal{J}_{eff}/\hbar^2 = T\left(\frac{\hbar^2}{\mathcal{J}_{\parallel}} - \frac{\hbar^2}{\mathcal{J}_{\perp}}\right)^{-1}. \qquad (2)$$

Here, T_ℓ denotes the probability of capture for the partial wave of angular momentum ℓ, $\mathcal{D}^{\ell}_{M=0,K}$ is the symmetric top wave function, T is the nuclear temperature, and $\mathcal{J}_{\parallel}$ and $\mathcal{J}_{\perp}$ are the transition state moments of inertia about axes of rotation parallel and perpendicular to the symmetry axis. From the systematics of Γ_n/Γ_f values [2,9] second chance fission is expected to be negligible for the systems $^{24}Mg+^{208}Pb$ and $^{28}Si+^{208}Pb$ and to contribute less than 30% to the fission cross section for the system $^{19}F + ^{208}Pb$. In equation 1, the intrinsic spin of ^{19}F, S = 1/2, is neglected. This is well justified because of the rather large entrance channel angular momenta.

Fission fragment angular distributions at energies close to the fusion barrier depend strongly on the distribution of the partial wave fusion probabilities T_ℓ, as discussed in detail in ref. 8. For the fits shown by the solid curves in Figure 1, we have used the relation [7,8]

$$T_\ell = T^{(OM)}_{\ell+\ell'} \qquad (3)$$

where $T_{\ell}^{(OM)}$ are transmission coefficients obtained from optical model fits to elastic scattering angular distributions that were simultaneously measured in this experiment. At each energy the parameter ℓ'

was adjusted to reproduce the experimental fission cross section. The angular momentum dependence of the effective moments of inertia was parameterized by the simple functional dependence [8] of the form

$$\mathcal{J}_o/\mathcal{J}_{eff} = \begin{cases} a - b\,\ell^2, & \text{for } \ell^2 \leq \frac{a-c}{b} \\ c, & \text{for } \ell^2 > \frac{a-c}{b} \end{cases} \quad . \qquad (4)$$

Here, we have used the rigid sphere moments of inertia (corresponding to the radius $R = 1.225\ A^{1/3}$ fm) to obtain the dimensionless numbers $\mathcal{J}_o / \mathcal{J}_{eff}$. For simplicity, the nuclear temperature was calculated from the simple relation $T = 7.7$ MeV E^*/A, which neglects the spin dependence of the nuclear temperature. The resulting fits are excellent. The best - fit values of $\mathcal{J}_o/\mathcal{J}_{eff}$ as a function of ℓ^2 are shown by the dashed lines in Figure 2 and the corresponding best fit parameters are listed in Table 2. Also included in the Figure are the results of a similar analysis [8] for the reaction $^{32}S + ^{208}Pb$. The extracted values of $\mathcal{J}_o/\mathcal{J}_{eff}$ are in clear disagreement with the saddle point shapes of the rotating liquid drop model which are shown by the solid curves. For all four cases investigated, the effective moments of inertia reach asymptotic values

$J_o/J_{eff} > 0.6$ at high angular momenta, corresponding to transition states of rather considerable deformations. At these large angular momenta the fission barriers are expected to vanish, and the reaction is expected to proceed via fast fission [10-12]. Our observations are in qualitative agreement with recent TDHF calculations performed for heavier systems which indicate that fast fission reactions proceed via rather deformed configurations [13] of the composite system. If, on the contrary, more compact configurations are reached for these reactions our results might indicate that fission fragment angular distributions are not sensitive to these compact configurations because of considerable rearrangement of the angular momentum projections prior to scission.

At energies close to the fusion barrier, rather broad distributions of the partial wave fusion probabilities are obtained from the prescription of eq. 3. Although recent measurements of gamma ray multiplicities [14] indicate that these broad distributions may, indeed, be justified it is still appropriate to present an analysis of the angular distributions in terms of the more conventional sharp cut-off model for the partial wave fusion cross sections. The two assumptions are then expected to bracket the "true" distribution of the partial wave capture cross sections. Fits of comparable quality as the ones shown in Figure 1 are obtained with the sharp cut-off approximation if one adopts

the simple parameterisation of eq. 4 or, alternatively, if one assumes a constant value of $\mathcal{J}_o/\mathcal{J}_{eff}$ for each energy. The resulting best - fit parameters are shown in Figure 2 by the dot - dashed lines and the solid bars, respectively. Clearly, the discrepancies with the saddle point shapes of the rotating liquid drop model become worse if the sharp cut-off approximation is used.

In conclusion, fission fragment angular distributions measured for ^{19}F, ^{24}Mg, ^{28}Si, and ^{32}S induced reactions on ^{208}Pb were analyzed in terms of the transition state model for nuclear fission. At low angular momenta, the extracted values of $\mathcal{J}_o/\mathcal{J}_{eff}$ decrease with increasing angular momentum of the composite nucleus in qualitative agreement with the expectations from the rotating liquid drop model. However, quantitative agreement between the measured and predicted values of $\mathcal{J}_o/\mathcal{J}_{eff}$ was not obtained for any of the cases investigated. The discrepancies between the extracted and predicted values of $\mathcal{J}_o/\mathcal{J}_{eff}$ are most pronounced for the heavier projectiles ^{28}Si and ^{32}S. These discrepancies indicate that the determination of angular momentum transfer in deeply inelastic reactions from measurements of fission fragment angular correlations may have considerable uncertainties unless the effective moments of inertia are established from independent measurements. Our measurements extend well into the region of angular momenta for which the fission barrier is expected to vanish. For these large angu-

lar momenta, the effective moments of inertia reach asymptotic values of $\mathcal{J}_o/\mathcal{J}_{eff} > 0.6$ corresponding to rather deformed transition states. At present it is not certain whether the extracted values of $\mathcal{J}_o/\mathcal{J}_{eff}$ are a property of the composite nucleus or whether they depend on the entrance channel. Additional measurements with different projectile target combinations will be necessary to elucidate this important question.

This work was supported by the U.S. Department of Energy and by the National Science Foundation under Grant No. 80-17605. One of us (C.K.G.) acknowledges the partial support of the Alfred P. Sloan Foundation.

References

1. A. Bohr, in Proceedings of the United Nations Intl. Conference on the Peaceful Uses of Atomic Energy, Geneva 1955 (United Nations, New York, 1956), Vol. 2, p. 151

2. R. Vandenbosch and J.R. Huizenga, Nuclear Fisson, Academic Press, New York (1973)

3. L.C. Vaz and J.M. Alexander, preprint 1983

4. S. Cohen and W.J. Swiatecki, Ann. Phys. 22 (1963) 406

5. S. Cohen, F. Plasil, and W.J. Swiatecki, Ann. Phys. 82 (1974) 557

6. B.B. Back, H.-G. Clerc, R.R. Betts, B.G. Glagola, and B.D. Wilkins, Phys. Rev. Lett. 46 (1981) 1068

7. B.B. Back, R.R. Betts, K. Cassidy, B.G. Glagola, J.E. Gindler, L.E. Glendenin, and B.D. Wilkins, Phys. Rev. Lett. 50 (1983) 818

8. M.B. Tsang, D.Ardouin, C.K. Gelbke, W.G. Lynch, Z.R. Xu, B.B. Back, R. Betts, S. Saini, P.A. Baisden, and M.A. McMahan, to be published in Phys. Rev. C.

9. K.-H. Schmidt, W. Faust, G. Münzenberg, W. Reisdorf, H.-G. Clerc, D. Vermeulen, and W. Lang, Physics and Chemistry of Fission 1979, International Atomic Energy Agency, Vienna, 1980, Vol.1, p.409

10. B. Borderie, M. Berlanger, D. Gardes, F. Hanappe, L. Nowicki, J. Péter, B. Tamain, S. Agarwal, J. Girard, C. Grégoire, J. Matuszek, and C. Ngô, Z. Phys. A299 (1981) 263

11. C. Grégoire, C. Ngô, and B. Remaud, Phys. Lett. 99B (1981) 17, and Nucl. Phys. A383 (1982) 392

12. W.J. Swiatecki, Physica Scripta 24 (1981) 113 and Nucl. Phys. A376 (1982) 275

13. H. Stöcker, R.Y. Cusson, H.J. Lustig, A. Gobbi, J. Hahn, J.A. Maruhn, and W.Greiner, Z. Phys. A3Ø6 (1982) 235

14. R. Vandenbosch, B.B. Back, S. Gil, A. Lazzarini, and A. Ray, University of Washington preprint, 1983

Figure captions.

Fig. 1. Fission fragment angular distributions measured for ^{19}F, ^{24}Mg, and ^{28}Si induced reactions on ^{208}Pb. The solid curves are the result of the global fits in terms of equations 1-4. The dashed lines show the limit of $d\sigma/d\Omega = 1/\sin\theta$.

Fig. 2. Angular momemtum dependence of $\mathcal{J}_o/\mathcal{J}_{eff}$ extracted from the analysis of the angular distributions. The dashed and dot - dashed lines are the results of the global fits with the parameterization of eq. 4, using eq. 3 and the sharp cut-off approxiation, respectively, for the partial wave fusion probabilities. The solid bars correspond to fits with a constant value for K_o at each energy; for these fits the estimated errors are indicated by the vertical bars and the lengths of the horizontal bars correspond to the range of angular momenta contibuting to the fission cross sections. The solid lines show the effective moments of inertia predicted by the rotating liquid drop model.

Table Captions

Table 1. Fission cross sections, σ_f, and sharp cut-off angular momenta for capture, ℓ_c.

Table 2. Best fit parameters corresponding to the parameterization of the effective moments of inertia in terms of eq. 4.

Table 1.

Reaction	ELAB (MeV)	σ_f (mb)	ℓ_c ($\hbar$)
$^{19}F+^{208}Pb$	110	689±35	41.9±1.1
	120	958±65	51.8±1.8
	135	1257±65	63.2±1.6
	150	1449±80	71.7±2.0
	170	1630±132	81.0±3.3
	190	1924±105	93.2±2.6
$^{24}Mg+^{208}Pb$	140	419±30	40.5±1.5
	145	570±29	48.3±1.3
	160	848±43	62.1±1.6
	170	1037±59	71.0±2.1
	190	1358±68	86.1±2.2
	210	1606±88	98.5±2.7
$^{28}Si+^{208}Pb$	160	309±22	39.5±1.5
	170	516±30	52.9±1.6
	180	747±39	65.7±1.8
	200	987±69	79.9±2.8
	220	1197±75	92.4±3.0
	240	1446±83	106.2±3.1
	260	1628±94	117.4±3.4

Table 2.

	SHARP CUT-OFF MODEL			SHIFTED OPTICAL MODEL		
Reaction	a	b	c	a	b	c
$^{19}F+^{208}Pb$	1.64	1.88×10^{-4}	.74	1.55	1.60×10^{-4}	.72
$^{24}Mg+^{208}Pb$	1.17	7.04×10^{-5}	.62	.99	4.10×10^{-5}	.66
$^{28}Si+^{208}Pb$	1.75	2.93×10^{-4}	.80	1.36	1.63×10^{-4}	.83
$^{32}S+^{208}Pb$	3.86	2.32×10^{-3}	1.01	2.20	6.60×10^{-4}	1.01

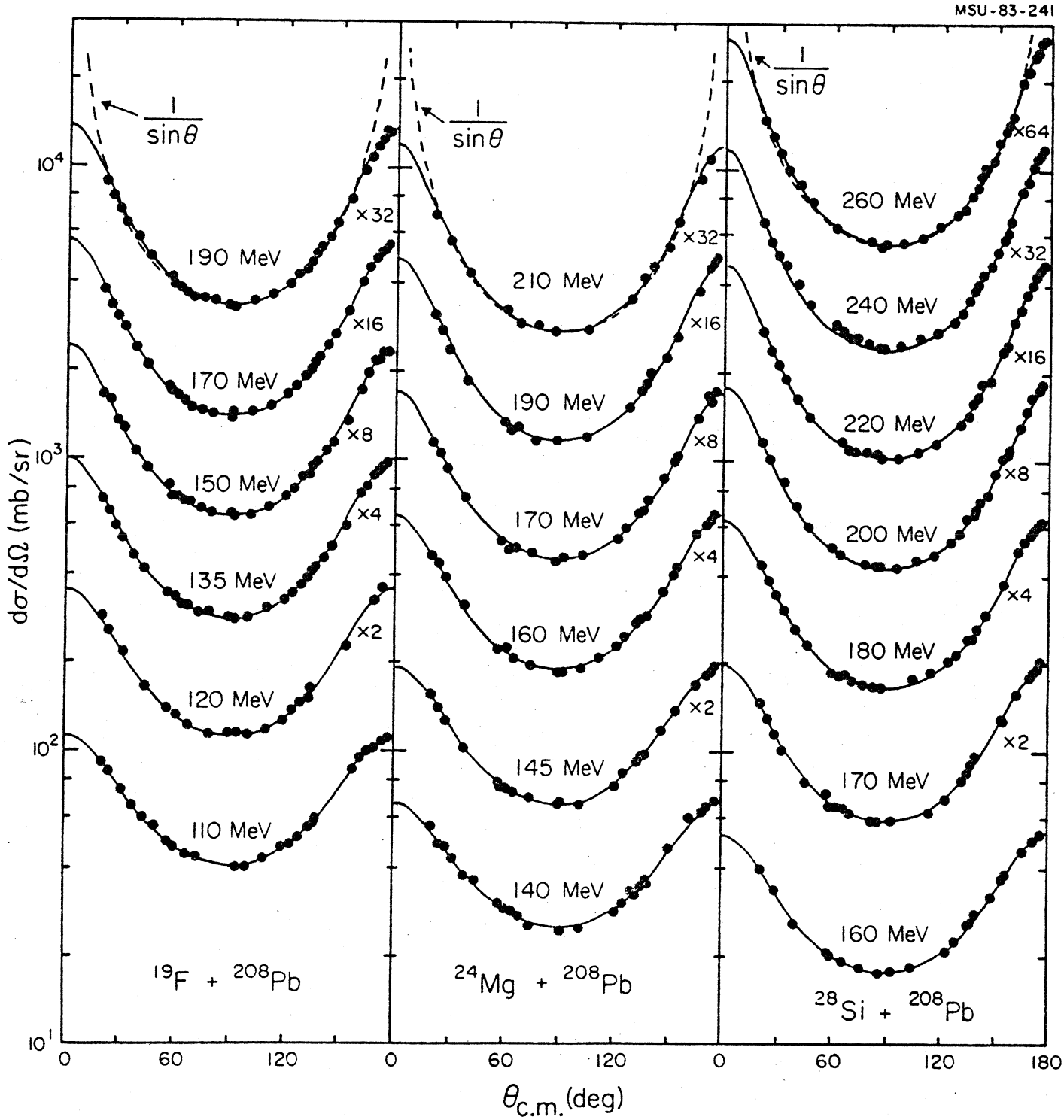
MSU-83-241
1/sinθ
190 MeV
170 MeV
150 MeV
135 MeV
120 MeV
110 MeV
210 MeV
190 MeV
170 MeV
160 MeV
145 MeV
140 MeV
260 MeV
240 MeV
220 MeV
200 MeV
180 MeV
170 MeV
160 MeV
×64
×32
×16
×8
×4
×2
$^{19}F + ^{208}Pb$
$^{24}Mg + ^{208}Pb$
$^{28}Si + ^{208}Pb$
dσ/dΩ (mb/sr)
10^4
10^3
10^2
10^1
0
60
120
180
$\theta_{c.m.}$(deg)

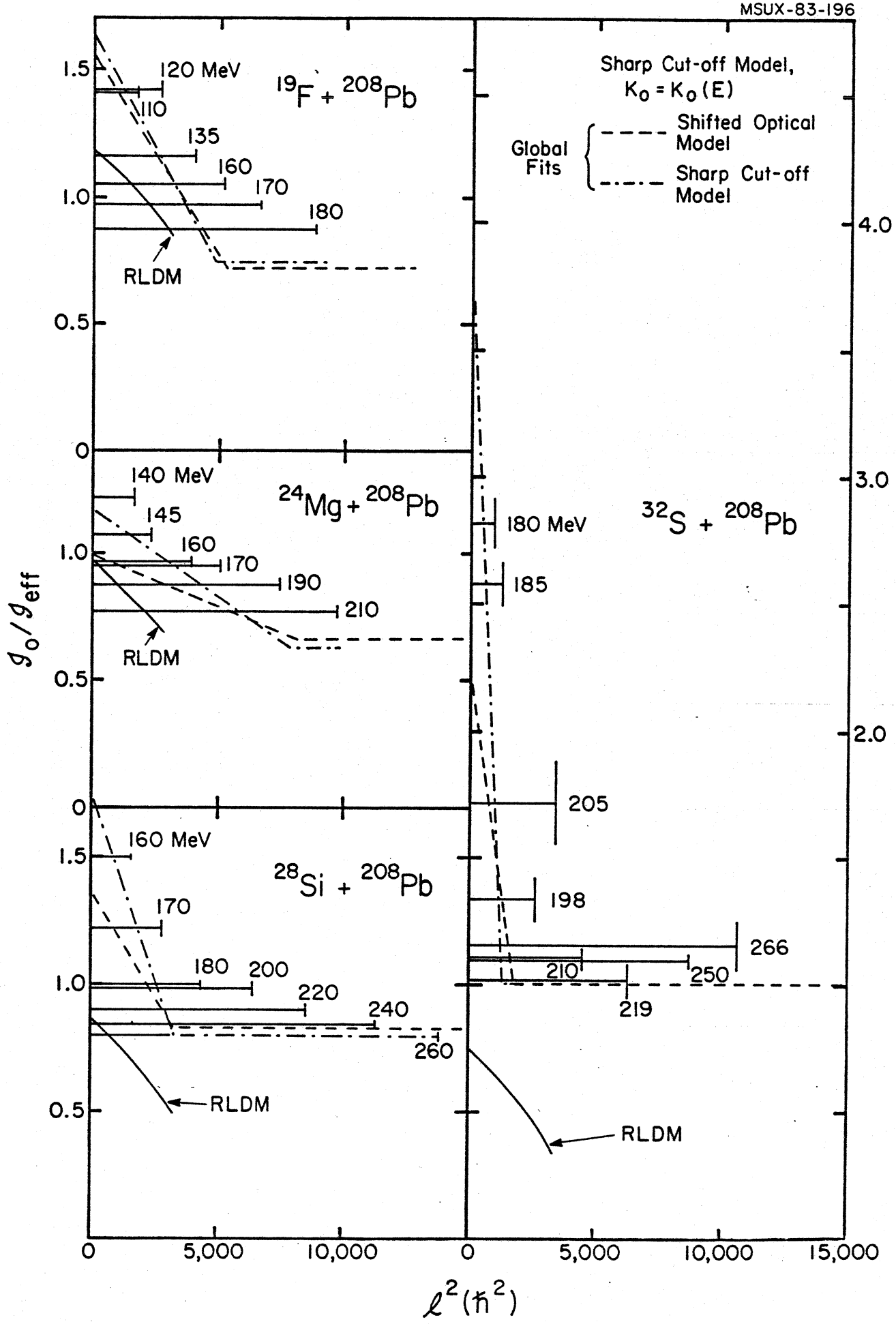
Sharp Cut-off Model,
$K_0 = K_0(E)$
Global Fits
Shifted Optical Model
Sharp Cut-off Model
$^{19}F + ^{208}Pb$
120 MeV
110
135
160
170
180
RLDM
$^{24}Mg + ^{208}Pb$
140 MeV
145
160
170
190
210
RLDM
$^{28}Si + ^{208}Pb$
160 MeV
170
180
200
220
240
260
RLDM
$^{32}S + ^{208}Pb$
180 MeV
185
205
198
266
210
250
219
RLDM
g_0/g_{eff}
$\ell^2(\hbar^2)$
0
5,000
10,000
15,000
0.5
1.0
1.5
2.0
3.0
4.0